In cellulo serial crystallography of alcohol oxidase crystals inside yeast cells

Arjen J. Jakobi[1,2#], Daniel M. Passon[1#], Kèvin Knoops[3], Francesco Stellato[4†], Mengning Liang[4‡], Thomas A. White[4], Thomas Seine[1,4], Marc Messerschmidt[5¶], Henry Chapman[4,6,7] and Matthias Wilmanns[1,8*]

[1] European Molecular Biology Laboratory (EMBL), Hamburg Unit c/o DESY, Notkestraße 85, 22607 Hamburg, Germany
[2] European Molecular Biology Laboratory (EMBL), Structural and Computational Biology Unit, Meyerhofstraße 1, 69117 Heidelberg, Germany
[3] Molecular Cell Biology, Groningen Biomolecular Sciences and Biotechnology Institute, University of Groningen, 9747 AG Groningen, The Netherlands
[4] Center for Free-Electron Laser Science, Deutsches Elektronen Synchrotron DESY, Notkestraße 85, 22607 Hamburg, Germany
[5] Linac Coherent Light Source, SLAC National Accelerator Laboratory, Menlo Park, California, USA
[6] Department of Physics, University of Hamburg, Luruper Chaussee 149, 22607 Hamburg, Germany
[7] Center for Ultrafast Imaging, Luruper Chaussee 149, 22607 Hamburg, Germany
[8] University Medical Center Hamburg-Eppendorf, Martinistraße 52, 20246 Hamburg, Germany

Current address:
[†] I.N.F.N. and Physics Department, University of Rome 'Tor Vergata', Via della Ricerca Scientifica 1, 00133 Rome, Italy
[‡] Linac Coherent Light Source, SLAC National Accelerator Laboratory, Menlo Park, California, USA
[¶] European XFEL, Albert-Einstein-Ring 19, 22761 Hamburg, Germany and National Science Foundation BioXFEL Science and Technology Center, 700 Ellicott Street Buffalo, New York 14203, USA

[#] These authors contributed equally to this work.
* Correspondence email: matthias.wilmanns@embl-hamburg.de.

Abstract

We have explored the possibility of using femtosecond pulses from an X-ray Free Electron Laser to collect diffraction data from protein crystals formed in their native cellular organelle. We report and characterize X-ray diffraction of submicrometer-sized alcohol oxidase crystals formed in peroxisomes within cells of genetically modified variants of the methylotrophic yeast *Hansenula polymorpha*. Our observations are supported by synchrotron radiation-based powder diffraction data and electron microscopy. Based on our findings, we outline a concept of *in cellulo* serial crystallography on protein targets imported into yeast peroxisomes without the need for protein purification as a requirement for subsequent crystallization.

Introduction

The recent advent of X-ray free electron lasers (XFELs) has led to rapid progress in determining three-dimensional structures from protein crystals only several hundreds of nanometers up to few micrometers in size and with diffracting volumes up to three orders of magnitude smaller than those commonly required for data collection at conventional synchrotron sources (Chapman et al., 2011; Boutet et al., 2012; Redecke et al., 2013). The use of XFEL radiation holds great promise to facilitate structure determination of protein species that have so far remained recalcitrant to structural characterization by X-ray crystallography due to the difficulty in forming well-ordered crystals of sufficient size. Recently developed serial femtosecond

crystallography (SFX) approaches enable the collection of diffraction data prior to the emergence of radiation-induced structural disorder (Boutet et al., 2012). The success of these experiments has inspired the adaption of serial data collection strategies at synchrotron sources (serial synchrotron crystallography, SSX) (Gati et al., 2014; Stellato et al., 2014) and sparked considerable interest in methods to obtain, detect and optimize protein nanocrystals (Georgieva et al., 2006; Gualtieri et al., 2011; Kupitz et al., 2014; Stevenson et al., 2014).

The observation that protein crystals may form spontaneously within cells or cell organelles (Doye & Poon, 2006), however, has not been widely explored to date. Recent advancements in sample delivery and data collection approaches have made it possible to perform a number of proof-of-principle X-ray diffraction experiments on such samples at third-generation synchrotrons (Coulibaly et al., 2007; 2009; Axford et al., 2014; Gati et al., 2014) and XFELs (Koopmann et al., 2012; Sawaya et al., 2014; Ginn et al., 2015). These studies have provided an incentive for seeking strategies to systematically exploit cellular systems to produce protein crystals for SFX or SSX experiments (Koopmann et al., 2012; Gallat et al., 2014; Tsutsui et al., 2015). However, successful applications of *in cellulo* protein crystallization to determine novel protein structures are still pending to date.

A primary cellular compartment in which the formation of protein crystals *in cellulo* has been reported is the peroxisome. Peroxisomes are membrane-limited organelles in eukaryotic cells with important roles in sequestered lipid metabolism and the scavenging of reactive oxygen species (Wanders & Waterham, 2006). Crystal formation of peroxisomal enzymes has been observed in a range of organisms: alcohol oxidase in yeast peroxisomes (van Dijken et al., 1975; Tanaka et al., 1976; Veenhuis et al., 1978), uricase in rat hepatocyte peroxisomes (Hruban & Swift, 1964; Tsukada et al., 1966) and catalase in plant peroxisomes (Heinze et al., 2000). Here, we set out to assess the potential of SFX for solving the crystal structure of such enzymes in their native environment inside the cell.

We focused on *Hansenula polymorpha* (Hp), in which the predominant peroxisomal protein, alcohol/methanol oxidase (AO), has been observed to form submicron-sized crystals inside the peroxisomal matrix (Veenhuis et al., 1978; 1981). AO expression in methylotrophic yeast cells is strictly regulated at the transcriptional level by methanol induction. If grown on methanol as the main carbon source, the peroxisomal lumen is abundant in AO, which assembles into a crystalline matrix (**Figure 1a–b**). Hp-AO is a member of the glucose-methanol-choline oxidoreductases

and catalyzes the oxidation of methanol to formaldehyde with the concomitant production of hydrogen peroxide. Unlike most other oxidoreductases, peroxisomal Hp-AO in its mature form consists of eight identical subunits with a total molecular weight of approximately 600 kDa. X-ray diffraction of large Hp-AO crystals grown from purified protein was found to be limited to 6 Å, but no further characterization was reported (van der Klei et al., 1989). Despite historic efforts a Hp-AO crystal structure remains pending to date, the closest homolog of known structure being monomeric pyridoxine 4-oxidase (PDB ID 4ha6) with 29.4% sequence identity. Owing to the small overall dimensions of Hp peroxisomes the experimental conditions of hard X-ray FELs are well suited for diffraction experiments with this challenging target. Here we demonstrate that SFX diffraction up to 6 Å resolution can be observed from single micrometer-sized peroxisomal AO crystallites within their native environment in intact yeast cells.

Results

To assess the suitability of peroxisomes as a source of nanocrystals for SFX experiments, we first purified and characterized peroxisomes from NCYC495 wild-type *(wt)* Hp yeast cells (Sudbery et al., 1988) as well as mutant strains deficient in PEX11 (Krikken et al., 2009) and PEX5 genes (Salomons et al., 2001). Genetic knock-out of PEX5 (Δ*PEX5*) results in a dysfunctional peroxisomal import pathway (van der Klei et al., 1991). Strains deficient in the PEX11 gene (Δ*PEX11*) display impaired peroxisome proliferation (fission) and commonly contain only a single peroxisome per cell (Krikken et al., 2009) (**Figure 1c**).

We exploited the use of Δ*PEX11* cells to alleviate the potential problem of obtaining multiple and overlapping diffraction patterns from individual Hp cells, which despite the small beam diameter (100-300 nm) can represent a serious detriment if two or more crystals located along the beam direction interact simultaneously with a single X-ray pulse. To assess the level of sample homogeneity of *wt* and Δ*PEX11* cells, we quantified peroxisome number and size inside cells in parallel by fluorescence microscopy. We fused the adenosine triphosphate transporter Pmp47 to a monomeric mutant of green-fluorescent protein (Pmp47-mGFP; **Figure 1d–e**) to label and measure the peroxisomal membrane outlining the AO crystals. On average, Δ*PEX11* cells contained slightly larger peroxisomes (0.88 ± 0.55 µm) than *wt* cells (0.70 ± 0.24 µm). The distribution of peroxisome size is more uniform in *wt* cells than the Δ*PEX11* variant, with only a small proportion of peroxisomes having dimensions larger than one micrometer. The narrow size distribution with an average diameter of

approximately 700 nm suggests that expected experimental errors of diffraction data resulting from sample size inhomogeneity (Kirian et al., 2010) are relatively low. These results are confirmed by dynamic light scattering data obtained with isolated peroxisome fractions that were purified from the host cells (**Figure 1f**). In Δ*PEX11* cells a significant fraction of peroxisomes grew extraordinarily large approaching a diameter of ~2.5 µm. This size increase is explained by the preservation of total peroxisomal volume in Δ*PEX11* cells, which accumulates in a single peroxisome. Since the diffraction signal is expected to scale with the illuminated crystal volume, we tried to further enrich for Δ*PEX11* cells with large peroxisomes by fractional centrifugation on a sorbitol cushion. Gradient fractionation resulted in a marked reduction of the cell population with small peroxisomes and a moderate increase of cells with very large peroxisomes (1.1 ± 0.62 µm) relative to the untreated sample (**Figure S1**). Finally, to assess the importance of compartmentalization (in addition to size) for crystal quality, we also investigated Δ*PEX5* cells with impaired peroxisomal import. In this mutant, we expect to find AO crystals only in the cytosol (van der Klei et al., 1991), hence allowing the comparison with crystals grown inside peroxisomes to yield a quantitative assessment of the effect of organelle confinement on diffraction quality.

We induced formation of crystalline AO by growing *Hp* cells on methanol-containing medium and tested the diffraction properties of concentrated cell and organelle suspensions at the EMBL/DESY beamline P14 at the PETRA-III synchrotron. For all preparations we observed visible Debye-Scherrer rings extending to ~40 Å, suggesting that all cells and purified peroxisomes investigated comprised a crystalline state of the AO matrix (**Figure 2a–d**). The observed *d*-spacings in the diffraction data are compatible with an *I*-centered cubic lattice and a cell edge of ~228 Å. Of note, reflections 211, 220 and 222 are not visible in the diffraction data. The lattice constants inferred from the powder diffraction data are supported by distances in Fourier amplitude spectra calculated from electron micrographs of crystalline AO in peroxisomes in our sample preparation (**Figure S2**). These dimensions are in agreement with previous electron diffraction data from AO crystalloids grown *in vivo* (Veenhuis et al., 1981) or from purified protein (Vonck & van Bruggen, 1992). Debye-Scherrer rings are strongest for the *wt* and Δ*PEX11* preparations and significantly weaker for Δ*PEX5* cells (**Figure 2b–d, Figure S3**). Purified peroxisomes from *wt* cells produce the same diffraction patterns as observed for whole cells suspensions (**Figure 2e**), whereas reflections are absent in cell

suspensions of an Δ*AO* strain (Lahtchev et al., 2002) in which Hp-AO expression is abrogated (**Figure 2f**). In summary, these experiments confirm detection of X-ray diffraction from crystalline AO in purified peroxisomes as well as *wt*, Δ*PEX11* and Δ*PEX5* cells with intensities of Debye–Scherrer signals that are well beyond background levels.

Next, we tested diffraction from AO crystallites in individual cells at the coherent X-ray imaging (CXI) experiment at the Linac Coherent Light Source (LCLS). We first optimized conditions for introducing peroxisome and yeast cell suspensions into the X-ray beam as a thin liquid jet using a gas dynamic virtual nozzle (GDVN) (DePonte et al., 2008). We purified the peroxisomes on isosmotic sucrose gradients and initially stored them in high percentage sucrose buffers as previously described (Graham, 2001). During test runs with our buffer solutions on a GDVN replica setup it became apparent that high percentage sucrose solutions did not produce stable jets due to rapid nozzle clogging. We therefore substituted the sucrose buffer with an isosmotic solution of 1.5 M sorbitol (Weast et al., 1986), which we could jet successfully with a GDVN nozzle. Yeast cells could be re-suspended in phosphate buffer or distilled water without compromising their integrity or the diffraction properties of crystalline AO. In our experiments we used a nozzle of 50 µm inner diameter with a liquid flow rate of ~ 15 µl/min to produce a stable jet of ~5 µm diameter for the whole cell and peroxisome suspensions. Diffraction patterns were obtained by exposing a fully hydrated stream of cells to X-ray pulses of nominal 30 fs duration and recorded on a Cornell-SLAC pixel array detector (CSPAD) at a frequency equal to the X-ray pulse rate (120 Hz). We collected a total of 309,496 frames for Δ*PEX11* cell suspensions and 43,056 frames for Δ*PEX5* cells. Hit finding procedures using Cheetah (Barty et al., 2014) characterized a total of 3404 (1.1%) patterns as single crystal diffraction for the Δ*PEX11* cells. For Δ*PEX5* cells, 215 (0.5%) single crystal diffraction patterns were found. The scarcity, as well as the very low resolution and poor overall quality of the Δ*PEX5* data did not permit any further processing.

Inspection of individual Δ*PEX11* images revealed well-resolved Bragg-sampled diffraction patterns, indicating single crystal diffraction (**Figure 3a**). Owing to the low resolution, however, single images contained too few Bragg peaks to be indexed robustly by CrystFEL or *cctbx.xfel* (White et al., 2012; Sauter et al., 2013). For overall comparison of the SFX data and the X-ray powder diffraction (XRPD) patterns

collected at the PETRA-III synchrotron, we therefore generated composite powder patterns by summing all individual SFX diffraction images that contain Bragg peaks. The limited number of diffracting crystallites led to incompletely sampled, but discernible Debye-Scherrer rings in the composite powder patterns (**Figure 3b**). While the majority of diffraction patterns are restricted to approximately 30 Å, we occasionally observed diffraction up to the detector edge at 6.0 Å (**Figure 3c–d**) thus suggesting that the highest attainable resolution was possibly limited by the experimental geometry. From the size distribution of the Δ*PEX11* peroxisomes (**Figure 1e**) and the lattice constants derived from the diffraction data we estimate that crystals intercepting the X-ray pulses consist of approximately 10,000 (0.5 µm; 0.125 µm^3) to 1,300,000 (2 µm; 8 µm^3) unit cells, with only 700 to 24,000 unit cells contained in the illuminated crystal volume assuming a centered beam crossing and a beam cross section of 0.016 to 0.14 µm^2. Assuming one or two molecules per asymmetric unit as deduced from electron microscopy (Vonck & van Bruggen, 1992), we estimate the solvent content in the putative *I*-centered cubic lattices as 63%, 75% or 82%. This figure is significantly larger than for structures solved from similarly small crystals (Chapman et al., 2011; Sawaya et al., 2014, Ginn et al., 2015) and could present one reason why high resolution diffraction of AO crystals has been impossible to obtain to date.

Discussion

We demonstrate that SFX is able to detect *in cellulo* distinct diffraction properties of a large protein complex – octameric Hp-AO – crystallized in its native cellular compartment. Hp-AO has not been amenable to high-resolution structure determination to date, despite substantial efforts both by electron microscopy and X-ray crystallography (Veenhuis et al., 1981; Van der Klei et al., 1989; Vonck & van Bruggen, 1990), and therefore presents a challenging protein target for structure determination. Assuming that previously grown Hp-AO crystals (van der Klei et al., 1989) were at least 100 µm in size (no details were reported in (van der Klei et al., 1989)), the *in vivo* grown crystallites used here contained a fraction of only 1/10^6 unit cells or less given an estimated size of approximately 1 µm or less. Hence, we believe that it has been a significant milestone to achieve a comparable resolution limit of 6 Å for such a challenging sample with SFX.

In cellulo crystallization in peroxisomes as we have presented here, in principle allows the use of either isolated peroxisomes or entire yeast cells with intracellular

peroxisomes. The latter is intuitively expected to increase the background scatter substantially as a result of additional scattering components from non-peroxisomal cell material including membranes and cell wall. Perhaps surprisingly therefore, our powder diffraction data obtained with isolated peroxisomes and whole yeast cells suggest that scattering of other cellular components does not detrimentally affect data quality. This is in line with findings reported by others (Axford et al., 2014; Sawaya et al., 2014). On the other hand, increased mechanical stability of entire yeast cells may present an advantage in view of the experimental conditions required for sample preparation and sample delivery for SFX data acquisition. We made use of a genetically modified Hp variant, Δ*PEX11,* which impairs peroxisome fission to avoid the presence of overlapping diffraction patterns from crystalline material in different peroxisomes that are simultaneously interacting with the X-ray beam. The use of Δ*PEX11* cells has the additional advantage of allowing optimization of growth conditions such that an overwhelming proportion of the yeast cell cytoplasm is filled with crystalline material from a single peroxisome, thus increasing the diffraction signal.

Another variant – leading to a cell phenotype where AO crystals form in the cytosol due to dysfunctional Pex5-dependent cargo translocation – did not produce any useful diffraction data. A plausible explanation is the loss of favorable conditions for Hp-AO crystallization outside the peroxisomal lumen. Compartmentalization and directed import are likely to allow for substantially higher local protein concentration than can be reached by freely diffusing AO in the cytosol, and in addition present a natural ‘purification’ step separating the crystallization process from numerous contaminating proteins present in the cytosol. This is in agreement with previous data demonstrating that spatial confinement lowers the solubility threshold of protein solutions and positively affects their crystallization tendency (Tanaka et al., 2004).

With the aim to identify experimental conditions that sufficiently improve the diffraction of *in vivo* grown AO crystals to solve the Hp-AO structure we are working towards a systematic characterization of variations in experimental parameters such as modulation of growth conditions, improved yeast strains, diagnostic tools for crystal identification and characterization *in cellulo*, and different forms of sample delivery.

Our long-term goal is to exploit the amenability of Hp and other yeast strains to genetic manipulation for structural determination of various protein targets. Proteins tagged with a peroxisomal translocation signal (PTS) tripeptide at the carboxyl-terminus are translocated from the cytosol into the peroxisomal matrix (Purdue & Lazarow, 1994; Rachubinski & Subramani, 1995). Heterologous expression of target proteins with such a PTS signal under the strong AOX promoter in Δ*AO* strains may allow sorting and focally concentrating the protein of interest into peroxisomes for crystal formation. In principle, adjusting growth conditions provides the possibility to control the rate of protein expression, subcellular sorting or the rate of peroxisomal import and thereby influence the extent of supersaturation and the rate of crystal growth *in vivo*. The lessons learned from the present study will help to address important experimental challenges lying ahead for intracellular crystal formation and its exploitation for structure solution of biological macromolecules. Our results provide a promising starting point to foster efforts aimed at developing *in cellulo* crystallization into a useful alternative to other crystallization strategies.

Acknowledgements

We thank Chris Williams (University of Groningen) and Dana Komadina (EMBL Hamburg) for their contribution in the early stages of the project, Gleb Bourenkov (EMBL Hamburg) for help with XRPD data collection, Dominik Oberthür (Hamburg University) for DLS measurements and Antoine Schreurs (Utrecht University) for advice on EVAL software. The X-ray powder diffraction experiments were carried out at beamline P14 operated by the European Molecular Biology Laboratory (EMBL) at the PETRA III synchrotron source at the German Electron Synchrotron (DESY) in Hamburg, Germany. Parts of this research were carried out at the Linac Coherent Light Source (LCLS) at the SLAC National Accelerator Laboratory. LCLS is an Office of Science User Facility operated for the US Department of Energy Office of Science by Stanford University. M.M was supported by NSF award 1231306, K.K. by Marie-Skłodowska-Curie IEF grant (FP7-IEF-330150). A.J.J. acknowledges support by an EMBL Interdisciplinary Postdoc (EIPOD) fellowship under Marie-Skłodowska-Curie COFUND Actions (PCOFUND-GA-2008-229597) and Marie-Skłodowska-Curie IEF grant (PIEF-GA-2012-331285). M.W. and H.C. acknowledge the support by the Hamburg Center for Ultrafast Imaging.

Material and Methods

H.polymorpha growth conditions

Yeast cultures were pre-cultured at 37°C in mineral media (van Dijken et al., 1976) supplemented with 0.5% glucose. For AO induction, the cells were shifted into mineral media containing 0.5% methanol as the carbon source at an OD_{600} of 0.1 and grown for 16h at 37°C. If required uracil and/or leucine were added to a final concentration of 30 µg/ml.

Organelle purification

The peroxisome organelle purification was performed with 4 L of methanol-grown cultures. The harvested cells were converted into protoplasts using Zymolase 20T (van der Klei et al. 1998) and homogenized. Peroxisomes were isolated by differential and sucrose density centrifugation and confirmed by western blot with antibodies against the peroxisomal marker alpha PEX11 (Douma et al. 1985). The enriched peroxisomal fraction were diluted with 1.5 M sorbitol in 5 mM MES pH 5.5, 0.1 mM EDTA, 1 mM KCl and 1 mM phenylmethylsulfonyl fluoride (PMSF) to a final concentration of 0.75 M sorbitol and 20% to 25% sucrose. A final buffer exchange was conducted by centrifugation at 30,000g for 30 mins and resuspension of the organelle pellet in1.5 M sorbitol, 5 mM MES pH 5.5, 0.1 mM EDTA, 1 mM KCl and 1 mM PMSF. The sample concentration was estimated with a counting chamber to 2 x 10^{11} particles mL^{-1} and stored at 4°C.

Fluorescence Microscopy

Fluorescent microscopy images of *wt* and ∆*PEX11* containing mGFP-tagged Pmp47 were captured with a confocal microscope (LSM510; Carl Zeiss), equipped with photomultiplier tubes (Hamamatsu Photonics) and Zen 2009 software. mGFP fluorescence was analyzed by excitation of the cell with a 488-nm argon ion laser (Lasos), and emission was detected using a 500–550 nm band-pass emission filter. For quantification of peroxisome sizes, Z stacks were acquired with an interval of 0.6 µm and analyzed using an ImageJ plugin (Williams et al., 2015). The presented images were created by median filtering the stacks in 3D (2x2x2 kernel) and merging in Z-direction by averaging.

Dynamic light scattering

Serial in situ DLS measurements were performed with a dilution of the purified peroxisome solution with a SpectroSize 300 (XtalConcepts, Germany) in a quartz cuvette with 7 µl sample volume (Hellma, Germany). The laser wavelength was set to 660 nm, 100 mW, the scattering angle of the detector placement to 90º. The dynamic viscosity parameter for sample buffer containing 1.5 M sorbitol was

calibrated using 600 nm NIST standard polystyrene microspheres (Duke Scientific). A dynamic viscosity parameter of 2.13 cP and refractive index of 1.33 were used for the experiment. A series of measurements (n=20, 300 ms) were directly recorded after pipetting at 293 K.

Electron microscopy

H. polymorpha wt cells were cryo-fixed in liquid ethane using the sandwich plunge freezing method (Baba, 2008). Cells were freeze-substituted in 1% osmium tetroxide, 0.5% uranyl acetate, and 5% (v/v) distilled water in acetone using the fast low-temperature dehydration and fixation method (McDonald & Webb, 2011). Cells were infiltrated overnight with Epon and polymerized for 48 h at 60 °C. 200-nm-thick sections were cut and overlayed with 10 nm of fiducial gold particles. Two single-axis tilt series, each containing 131 images with 1° tilt increments, were acquired on a FEI Tecnai20 running at 200 kV using the FEI automated tomography acquisition software and a cooled slow-scan charge-coupled device camera (Ultrascan 4000; Gatan) in 2×2 binned mode with a final pixel size of 1.1 nm at the specimen level. The tilt series were aligned and reconstructed by the simultaneous iterative reconstruction technique (SIRT) algorithm using the IMOD software package (Kremer et al., 1996).

X-ray powder diffraction

Cell suspensions of *wt*, Δ*PEX5*, Δ*PEX11* or Δ*AO* strains were concentrated to ~ $5x10^9$ cell/mL, transferred to a 0.1 mm glass capillary and pelleted. Capillaries were mounted on a vertically mounted goniometer of the MD3 microdiffractometer (EMBL/Bruker ASC/Arinax) at the P14 beamline at the PETRA III synchrotron (DESY, Hamburg) and powder patterns were collected on a Dectris Pilatus 6M detector using an exposure time of 10 s (10^{14} photons/sec). Diffraction data were visualized and analyzed with EVAL15 (Schreurs et al., 2009).

XFEL

SFX experiments were performed at the Coherent X-ray Imaging (CXI) beamline (Boutet et al., 2015) at the Linac Coherent Light Source (LCLS) using a tiled 2D pixel array detector (PAD). Data were collected from a fully hydrated stream of Δ*PEX11* and Δ*PEX5* cell suspensions at ~ $5x10^9$ cell/mL that were fixed prior to data collection. Cells were passed through a 10-µm stainless-steel frit mounted in-line with the sample tubing to prevent clogging of the injector. The samples were supplied to the

sample chamber as a gas-focused liquid jet of 5 µm diameter using a gas-dynamic virtual nozzle at a flow rate of ~ 15 µl min^{-1} at 20°C. To prevent settling of cells the suspension was agitated using a temperature-controlled anti-settling device (Lomb et al., 2012). Diffraction data were recorded using a 100-300 nm FWHM beam at a photon energy of 7.925 keV (1.56 Å) with 30 fs pulse duration. The CS-PAD detector was positioned at 425 mm from the sample interaction point. Diffraction patterns from AO crystals were identified and selected using the hit-finding program *Cheetah* (Barty et al., 2014). Composite powder diffraction patterns were assembled from the individual images using Cheetah and were visualized and analyzed using CrystFEL (White et al., 2012).

Figures

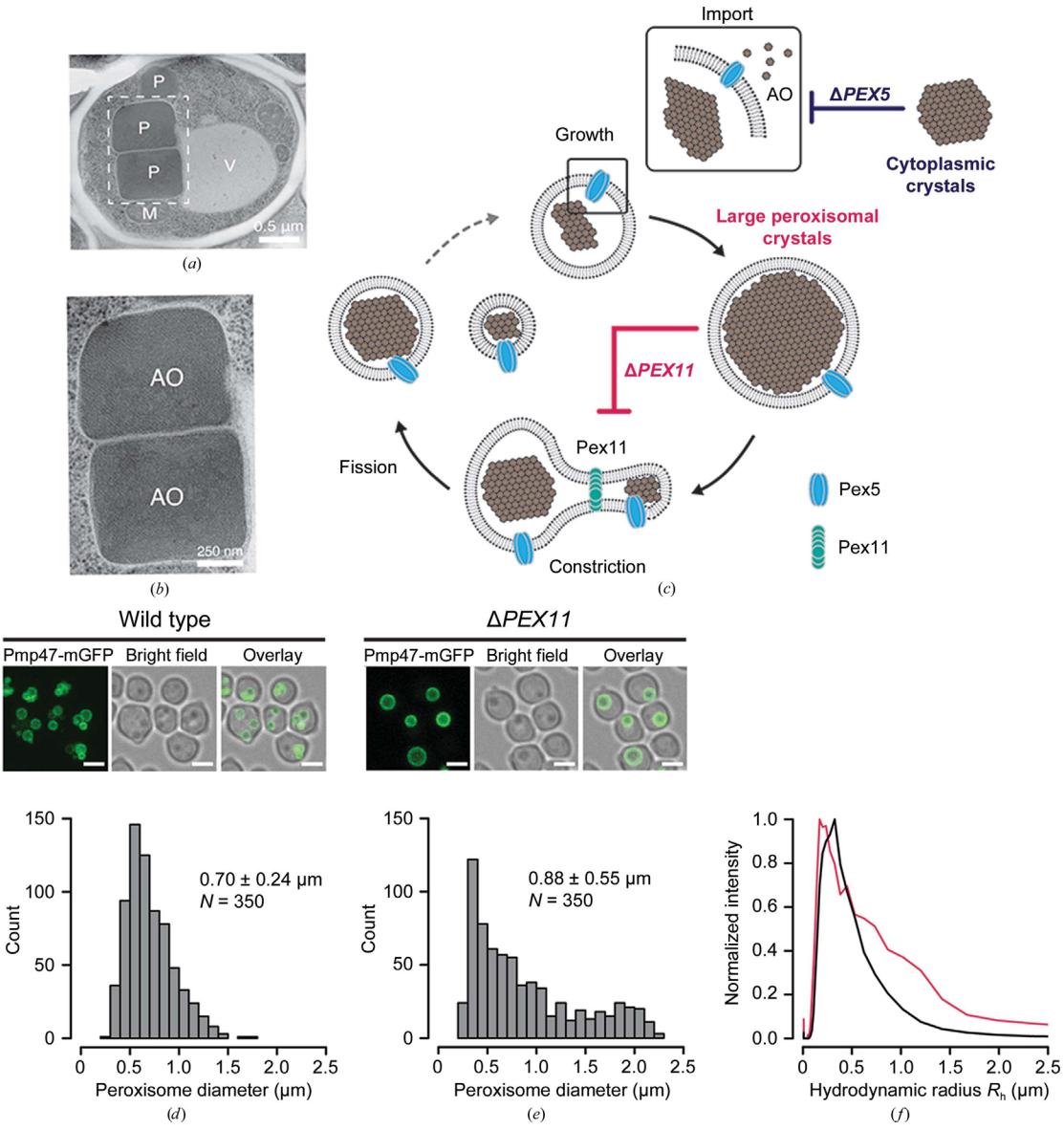

Figure 1 (a) Electron micrograph of *wt Hp* cell containing crystalline alcohol oxidase (AO) in electron-dense peroxisomes (P) seen next to mitochondria (M) and vacuole (V). The crystalline matrix is visible in the regular striated pattern observed at higher magnification (b). Also note the single membrane outlining the organelle and enclosing the crystal. (c) Schematic representation of peroxisome proliferation. Deletion of the cytosolic peroxisomal cargo receptor Pex5, which is also part of the peroxisomal translocon, prevents import of AO into the peroxisomal matrix and results in cytosolic AO crystals. (d–e) Δ*PEX11* cells display compromised fission and result in fewer (typically one) and larger peroxisomes per cell as seen by fluorescence microscopy with the peroxisomal membrane label Pmp47-mGFP. Scale bars are 2 µm. (f) Mean radius distributions from dynamic light scattering for purified fractions of *wt* (black) and Δ*PEX11* (red) peroxisomes.

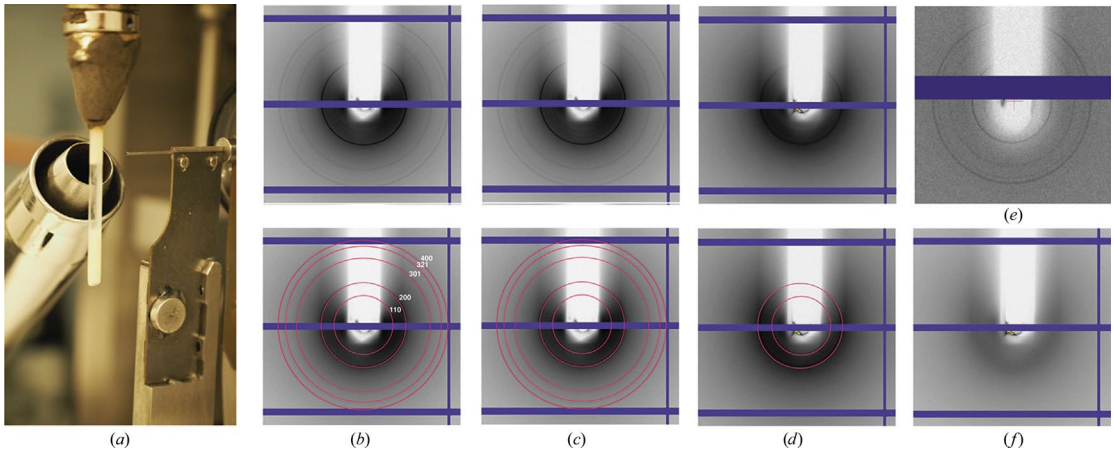

Figure 2 (a) Setup for powder diffraction experiments with cell and peroxisome suspensions at the P14 beamline at PETRA-III. X-ray powder diffraction patterns for (b) wild-type, (c) Δ*PEX11* and (d) Δ*PEX5* cells. Lower panels in (b–d) indicate Debye-Scherrer rings at 161 Å (corresponding to the 110 reflection), 114 Å (200 reflection), 72 Å (301 reflection) and 61 Å (321 reflection), consistent with *d*-spacings of an *I*-centred cubic lattice with *a* = 228 Å. Reflections 211, 220 and 222 are not visible in our diffraction data. (e) Purified peroxisomes produced the same diffraction pattern as wt and Δ*PEX11* cells, whereas Δ*AO* cells with a deletion in the AOX gene do not produce Debye-Scherrer rings (f).

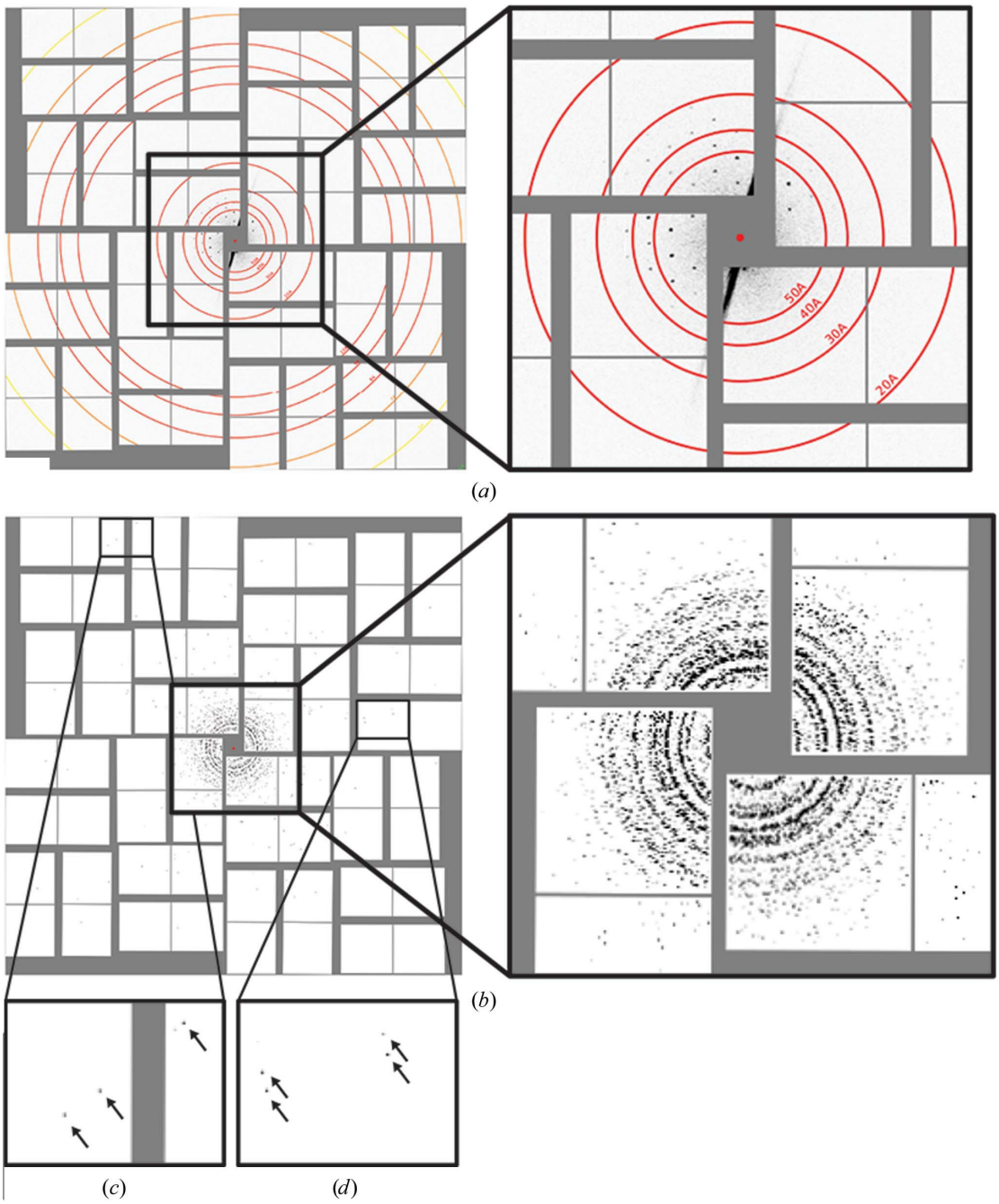

Figure 3 (a) Example SFX diffraction image of Δ*PEX11* cells displaying Bragg-sampled reflections with intensities above background level. (b) Composite XRPD patterns assembled from individual diffraction images show that most crystallites diffract to approximately 30 Å, with several crystals displaying diffraction out to the detector edge (6 Å) and corners (5.6 Å; insets c–d, arrows).

Supplementary Figures and Tables

Figure S1 (a) Brightfield and fluorescence images for total (top) and enriched (bottom) fractions of Δ*PEX11* cell suspensions. Scale bars represent 2 µm. (b) Size distribution of Pmp47-mGFP labeled Δ*PEX11* peroxisomes from enriched fractions of

∆*PEX11* cells show an increase in the fraction of very large peroxisomes (cf. Figure 1d–e).

Figure S2 (a) Representative digital electron tomogram slice of freeze-substituted AO crystallites in *Hp* peroxisomes with tetragonal arrangement of AO octamers viewed along [001]. (b) Fourier amplitude spectrum of (a) reflecting the discrete cubic lattice of AO in *Hp* peroxisomes.

Figure S3 X-ray powder diffraction patterns of (a) *wt*, (b) ∆*PEX11* and (c) ∆*PEX5* cells at higher threshold level than shown in Figure 2 (b–d) reveal additional, higher resolution Debye-Scherrer rings for *wt* and ∆*PEX11* cells (arrows).

References

Axford, D., Ji, X., Stuart, D. I., & Sutton, G. (2014). *Acta Crystallogr. D Biol. Crystallogr*. **70**, 1435–1441.

Baba, M. (2008). *Meth. Enzymol.* **451**, 133–149.

Barty, A., Kirian, R. A., Maia, F. R. N. C., Hantke, M., Yoon, C. H., White, T. A., & Chapman, H. (2014). *J Appl Crystallogr*. **47**, 1118–1131.

Boutet, S., Foucar, L., Barends, T. R. M., Botha, S., Doak, R. B., Koglin, J. E., Messerschmidt, M., Nass, K., Schlichting, I., Seibert, M. M., et al. (2015). *J. Synchrotron. Radiat*. **22**, 634–643.

Boutet, S., Lomb, L., Williams, G. J., Barends, T. R. M., Aquila, A., Doak, R. B., Weierstall, U., DePonte, D. P., Steinbrener, J., Shoeman, R. L., et al. (2012). *Science*. **337**, 362–364.

Chapman, H. N., Fromme, P., Barty, A., White, T. A., Kirian, R. A., Aquila, A., Hunter, M. S., Schulz, J., DePonte, D. P., Weierstall, U., et al. (2011). *Nature*. **470**, 73–77.

Coulibaly, F., Chiu, E., Gutmann, S., Rajendran, C., Haebel, P. W., Ikeda, K., Mori, H., Ward, V. K., Schulze-Briese, C., & Metcalf, P. (2009). *Proc. Natl. Acad. Sci. USA*. **106**, 22205–22210.

Coulibaly, F., Chiu, E., Ikeda, K., Gutmann, S., Haebel, P. W., Schulze-Briese, C., Mori, H., & Metcalf, P. (2007). *Nature*. **446**, 97–101.

DePonte, D. P., Weierstall, U., Schmidt, K., Warner, J., Starodub, D., Spence, J. C. H., & Doak, R. B. (2008). *J. Phys. D: Appl. Phys.* **41**, 195505.

Doye, J. & Poon, W. (2006). *Curr. Opin. Colloid Interface Sci.* **11***,* 40–46

Gallat, F.-X., Matsugaki, N., Coussens, N. P., Yagi, K. J., Boudes, M., Higashi, T., Tsuji, D., Tatano, Y., Suzuki, M., Mizohata, E., et al. (2014). *Philos. Trans. R. Soc. Lond., B, Biol. Sci.* **369**, 20130497.

Gati, C., Bourenkov, G., Klinge, M., Rehders, D., Stellato, F., Oberthür, D., Yefanov, O., Sommer, B. P., Mogk, S., Duszenko, M., et al. (2014). *IUCrJ*. **1**, 0–0.

Georgieva, D., Abrahams, J., & Kuil, M. (2006). *Springer Series in Biophysics*, J. Arrondo, & A. Alonso, edited by, pp. 1–25. Springer Berlin Heidelberg.

Ginn, H. M., Messerschmidt, M., Ji, X., Zhang, H., Axford, D., Gildea, R. J., Winter, G., Brewster, A. S., Hattne, J., Wagner, A., et al. (2015). *Nature Communications*. **6**, 6435.

Graham, J. M. (2001). *Curr Protoc Cell Biol*. **Chapter 3**, Unit3.5.

Gualtieri, E. J., Guo, F., Kissick, D. J., Jose, J., Kuhn, R. J., Jiang, W., & Simpson, G. J. (2011). *Biophys J*. **100**, 207–214.

Heinze, M., Reichelt, R., Kleff, S., & Eising, R. (2000). *Cryst. Res. Technol.* **35**, 877–886.

Hruban, Z. & Swift, H. (1964). *Science*. **146**, 1316–1318.

Kirian, R. A., Wang, X., Weierstall, U., Schmidt, K. E., Spence, J. C. H., Hunter, M., Fromme, P., White, T., Chapman, H. N., & Holton, J. (2010). *Opt. Express*. **18**, 5713–5723.

Koopmann, R., Cupelli, K., Redecke, L., Nass, K., DePonte, D. P., White, T. A., Stellato, F., Rehders, D., Liang, M., Andreasson, J., et al. (2012). *Nat Meth*. **9**, 259–262.

Kremer, J. R., Mastronarde, D. N., & McIntosh, J. R. (1996). *J Struct Biol*. **116**, 71–76.

Krikken, A. M., Veenhuis, M., & van der Klei, I. J. (2009). *FEBS J*. **276**, 1429–1439.

Kupitz, C., Grotjohann, I., Conrad, C. E., Roy-Chowdhury, S., Fromme, R., & Fromme, P. (2014). *Philos. Trans. R. Soc. Lond., B, Biol. Sci.* **369**, 20130316.

Lahtchev, K. L., Semenova, V. D., Tolstorukov, I. I., van der Klei, I., & Veenhuis, M. (2002). *Arch. Microbiol.* **177**, 150–158.

Lomb, L., Steinbrener, J., Bari, S., Beisel, D., Berndt, D., Kieser, C., Lukat, M., Neef, N., & Shoeman, R. L. (2012). *J. Appl. Crystallogr*. **45**, 674–678.

McDonald, K. L. & Webb, R. I. (2011). *J. Microsc*. **243**, 227–233.

Purdue, P. E. & Lazarow, P. B. (1994). *J. Biol. Chem*. **269**, 30065–30068.

Rachubinski, R. A. & Subramani, S. (1995). *Cell*. **83**, 525–528.

Redecke, L., Nass, K., DePonte, D. P., White, T. A., Rehders, D., Barty, A., Stellato, F., Liang, M., Barends, T. R. M., Boutet, S., et al. (2013). *Science*. **339**, 227–230.

Salomons, F. A., Nico Faber, K., Veenhuis, M., & Van der Klei, I. J. (2001). *J. Biol. Chem*. **276**, 4190–4198.

Sauter, N. K., Hattne, J., Grosse-Kunstleve, R. W., & Echols, N. (2013). *Acta Crystallogr. D Biol. Crystallogr*. **69**, 1274–1282.

Sawaya, M. R., Cascio, D., Gingery, M., Rodriguez, J., Goldschmidt, L., Colletier, J.-P., Messerschmidt, M. M., Boutet, S., Koglin, J. E., Williams, G. J., et al. (2014). *Proc. Natl. Acad. Sci. USA*. **111**, 12769–12774.

Schreurs, A. M., Xian, X., & Kroon-Batenburg, L. M. (2009). *J. Appl. Crystallogr*. **43**, 70–82.

Stellato, F., Oberthür, D., Liang, M., Bean, R., Gati, C., Yefanov, O., Barty, A., Burkhardt, A.,

Fischer, P., Galli, L., et al. (2014). *IUCrJ*. **1**, 204–212.

Stevenson, H. P., Makhov, A. M., Calero, M., Edwards, A. L., Zeldin, O. B., Mathews, I. I., Lin, G., Barnes, C. O., Santamaria, H., Ross, T. M., et al. (2014). *Proc. Natl. Acad. Sci. USA*. **111**, 8470–8475.

Sudbery, P. E., Gleeson, M. A., Veale, R. A., Ledeboer, A. M., & Zoetmulder, M. C. (1988). *Biochem. Soc. Trans.* **16**, 1081–1083.

Tanaka, A., Yasuhara, S., Kawamoto, S., Fukui, S., & Osumi, M. (1976). *J. Bacteriol.* **126**, 919–927.

Tanaka, S., Egelhaaf, S. U., & Poon, W. C. K. (2004). *Phys. Rev. Lett*. **92**, 128102.

Tsukada, H., Mochizuki, Y., & Fujiwara, S. (1966). *J. Cell Biol*. **28**, 449–460.

Tsutsui, H., Jinno, Y., Shoda, K., Tomita, A., Matsuda, M., Yamashita, E., Katayama, H., Nakagawa, A., & Miyawaki, A. (2015). *Mol. Cell*.

Van der Klei, I. J., Lawson, C. L., Rozeboom, H., Dijkstra, B. W., Veenhuis, M., Harder, W., & Hol, W. G. (1989). *FEBS Lett*. **244**, 213–216.

van der Klei, I. J., Lawson, C. L., Rozeboom, H., Dijkstra, B. W., Veenhuis, M., Harder, W., & Hol, W. G. J. (1989). *FEBS Lett*. **244**, 213–216.

van der Klei, I. J., Sulter, G. J., Harder, W., & Veenhuis, M. (1991). *Yeast*. **7**, 15–24.

van Dijken, J. P., Veenhuis, M., Kreger-van Rij, N. J., & Harder, W. (1975). *Arch. Microbiol.* **102**, 41–44.

Veenhuis, M., Dijken, J. P., Pilon, S. A. F., & Harder, W. (1978). *Arch. Microbiol.* **117**, 153–163.

Veenhuis, M., Harder, W., van Dijken, J. P., & Mayer, F. (1981). *Mol. Cell. Biol.* **1**, 949–957.

Vonck, J. & van Bruggen, E. F. (1990). *Biochim. Biophys. Acta*. **1038**, 74–79.

Vonck, J. & van Bruggen, E. F. (1992). *J. Bacteriol.* **174**, 5391–5399.

Wanders, R. J. A. & Waterham, H. R. (2006). *Annu. Rev. Biochem*. **75**, 295–332.

White, T. A., Kirian, R. A., Martin, A. V., Aquila, A., Nass, K., Barty, A., & Chapman, H. N. (2012). *J. Appl. Crystallogr*. **45**, 335–341.

Williams, C., Opalinski, L., Landgraf, C., Costello, J., Schrader, M., Krikken, A. M., Knoops, K., Kram, A. M., Volkmer, R., & van der Klei, I. J. (2015). *Proc. Natl. Acad. Sci USA*. **112**, 6377–6382.